Rocking Modes (Part 2: Diagnostics)

William Cardenas, Wolfgang Klippel; Klippel GmbH, Dresden 01309, Germany

The rocking behavior of the diaphragm is a severe problem in headphones, micro-speakers and other kinds of loudspeakers causing voice coil rubbing which limits the maximum acoustical output at low frequencies. The root causes of this problem are small imbalances in the distribution of the stiffness, mass and force factor in the gap. Based on lumped parameter modeling, modal decomposition and signal flow charts presented in a previous paper (Part 1) this paper here focusses on the practical measurement using laser vibrometry, parameter identification and root cause analysis. New characteristics are presented which simplify the interpretation of the identified parameters. The new technique has been validated by numerical simulations and systematic modifications of a real transducer. The diagnostic value of the new measurement technique has been illustrated on a transducer used in headphones.

0 INTRODUCTION

Most micro-speakers, headphones and some cone loudspeakers exhibit undesired rotational vibration patterns called rocking modes [3]. Rocking modes are caused by inhomogeneous distribution of mass, stiffness and force factor shifting the center of gravity, stiffness and electro-dynamical excitation away from the pivot point which is the cross point of the nodal lines of the two rocking modes. This imbalance generates moments exciting the rocking resonators to significant amplitudes. A detailed theoretical analysis and an extended lumped parameter model using three state variables (transversal displacement x_0, tilting angles τ_1 and τ_2) have been introduced in a previous paper [1].

This paper here focusses on the detection and identification of the root causes to provide meaningful information to eliminate the problem. Currently there are no diagnostic tools available for this purpose. The measurement of the mechanical vibration by laser scanning and post processing of the data by pressure related decomposition [2] and experimental modal analysis allow to separate the rocking behavior from the desired transversal vibration, but to provide no information on the magnitude and location of the imbalances. This paper is organized as follows: First, a short summary of the physical mechanisms and the consequences of each root cause are described based on the lumped parameter model presented in [1]. In the second chapter, the system identification, the experimental conditions of the measurement technique are explained and a set of meaningful characteristics which are easy to interpret are derived. In chapter three the measurement technique is evaluated by using numerical simulation (FEA) and practical experiments. The last chapter performs a rocking mode analysis on a headphone transducer to find the physical root causes and solve the problem in design and production processes.

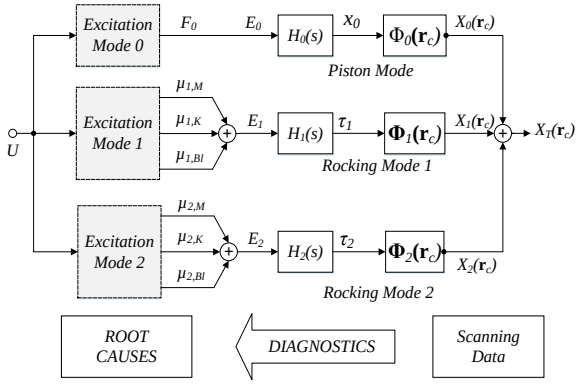

Fig 1. Signal flow chart representing the modal model

1. SUMMARY ON MODELING

The model presented in [1], explains the signal flow from the voltage U at the terminals to the displacement $X_T(\mathbf{r}_c)$ at any point $\mathbf{r}_c$ on the radiator's surface S_c as illustrated in Fig 1. This model comprises three parallel branches representing the fundamental piston mode (n=0) and the two rocking modes (n=1,2) with the corresponding modal state variables $\mathbf{x_L} = [x_0\ \tau_1\ \tau_2]^T$. The voltage U is converted into the modal excitation signal (force F_0) driving the fundamental resonator with the transfer function $H_0(s)$. The transversal displacement x_0 at the output of the resonator represents the state of the fundamental mode. Multiplying the modal amplitude x_0 with the mode shape $\mathbf{\Phi}_0$ gives the transversal displacement $X_0(\mathbf{r}_c)$ on the surface of the radiator. For each rocking mode (n=1,2), the input voltage can be converted into the moments $\mu_{n,E}$, with E ∈ {M,K,Bl} generated by the imbalances of mass, stiffness and force factor, respectively.

The total excitation signal E_n which is the sum of the three moments

$$E_n(s) = \mu_{n,M}(s) + \mu_{n,K}(s) + \mu_{n,Bl}(s) \qquad (1)$$

drives the rocking resonators with the transfer function $H_n(s)$ and produces the tilting angle τ_n. The tilting angle τ_n

gives in combination with mode shape $\mathbf{\Phi}_n$ the contribution of nth-order rocking mode to the total displacement $X_T(\mathbf{r}_c)$.

Only the total displacement $X_T(\mathbf{r}_c)$ can be measured by laser vibrometry and is the basis for the estimation of the lumped parameters. The identified model reveals the imbalances and gives access to all the forces and all moments $\mu_{n,E}$, with $E \in \{M,K,Bl\}$ and the modal state variables x_0, τ_1, τ_2.

2. PARAMETER IDENTIFICATION

The identification of the free parameters of the model requires a set of measurement points distributed on the diaphragm surface. The target is to extract the rigid body behavior of the driver exploiting the magnitude and phase of the displacement signal. Since the rocking mode is a low frequency mechanism, the frequency range needs to include enough frequency points in the frequency range $f_s/4 < f < 2f_s$ with the fundamental resonance frequency f_s of the transducer. The applied excitation voltage should be constant for all the excitation frequencies driving the loudspeaker in the linear operation range. In the future papers the effect of the imbalances of the nonlinear stiffness and force factor will be address.

2.1 Measurement setup

Theoretically, three measurement points are sufficient for describing the rotational and translational behavior of the diaphragm. In practice a large number of points is used (50-200) to ensure sufficient signal to noise ratio and to cope with optical errors. The length of the stimulus should be long enough to ensure sufficient frequency resolution to measure the peaky resonance curve caused by the high quality factor ($Q_n > 20$) of the rocking modes. A typical scan performed with a triangulation laser can be accomplished in less than 15 minutes. A linear parameter measurement (LPM) provides the T/S parameters of the electromechanical model.

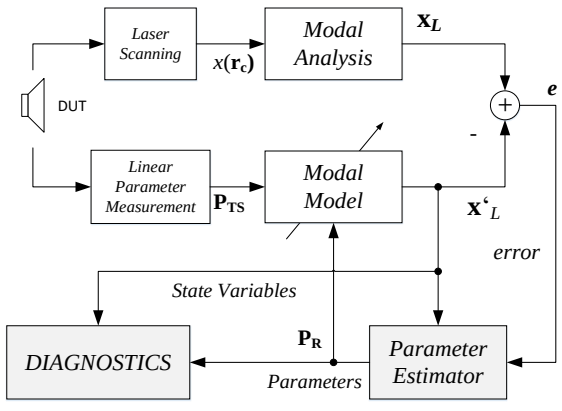

Fig 2. Measurement of the free parameters of the modal model

2.2 Parameter Identification

The identification scheme used for the estimation of the free model parameters is shown in Fig 2. The modal analysis generates the modal state variables $\mathbf{x_L} = [x_0\ \tau_1\ \tau_2]^T$ based on laser scanning data $x(\mathbf{r}_c)$. The modal model generates based on the linear lumped (T/S) parameters $\mathbf{P}_{TS}$ representing the fundamental mode and initial values of the additional lumped parameters $\mathbf{P_R}[0]$ describing the rocking modes (n=1,2) and estimated state variables $\mathbf{x'_L} = [x'_0\ \tau'_1\ \tau'_2]^T$. The optimal parameters $\mathbf{P_R}$ are determined iteratively by minimizing the error vector $\mathbf{e} = \mathbf{x_L} - \mathbf{x'_L}$. The identified state $\mathbf{x'_L}$ and parameters $\mathbf{P_R}$ and $\mathbf{P_{TS}}$ are the basis for the following transducer diagnostics.

3. CHARACTERISTICS

To simplify the interpretation of the state and parameter information additional characteristics are derived which reveal the root causes, the excitation of the modal resonators and the contribution to the displacement quantitatively.

3.1 Root Causes

The root causes of the rocking modes are small imbalance in the mass, stiffness and force factor distribution. This imbalance occurs if the center point of the distribution is not in the nodal cross point (pivot point) of the two rocking modes which is in the origin of the Cartesian coordinate system. The coordinates of the center of gravity can be expressed as

$$\begin{aligned} y_{CG} &= \Delta_{1,M} / M_{ms} \\ z_{CG} &= \Delta_{2,M} / M_{ms} \end{aligned} \tag{2}$$

using the coupling parameters $\Delta_{n,M}$ with n=1,2 of the identified modal model and the total moving point mass M_{ms} as introduced in [1].

The center of the stiffness is located at

$$\begin{aligned} y_{CK} &= \Delta_{1,K} / K_{ms} \\ z_{CK} &= \Delta_{2,K} / K_{ms} \end{aligned} \tag{3}$$

using the stiffness coupling $\Delta_{n,K}$ and the mechanical stiffness K_{ms}.

The center of the force factor is located at

$$\begin{aligned} y_{CBl} &= \Delta_{1,Bl} / Bl \\ z_{CBl} &= \Delta_{2,Bl} / Bl \end{aligned} \tag{4}$$

using parameters $\Delta_{n,Bl}$ and the transducer force factor Bl. The distance

$$d_E = \sqrt{y_{CE}^2 + z_{CE}^2} \qquad \mathrm{E} \in \{\mathrm{M,K,Bl}\} \tag{5}$$

between this center point and the origin shows the magnitude of the imbalance and the angle

$$\gamma_E = \arctan\left(\frac{y_{CE}}{z_{CE}}\right) + \gamma_0 \quad \mathrm{E} \in \{\mathrm{M,K,Bl}\} \tag{6}$$

reveals the direction of the imbalance whereas the constant γ_0 considers the orientation of the scanning grid. These parameters are close descriptors of the physical root causes but they do not consider the excitation condition of the

modal resonators which depends on the location of the resonance frequencies f_n with n=1,2 of the rocking modes and fundamental resonance frequency f_s of the piston mode, which determines the excitation moment.

3.2 Relative Rocking Level $RRL_{n,E}$

To assess the relevance of the rocking behavior it is useful to analyze first the total displacement $X(\mathbf{r}_c)$ on the radiator's surface S_c and to compare the amplitude of the undesired rocking modes with the amplitude of the desired piston mode. The relative rocking level

$$RRL_{n,E}(f_n) = AAL_{n,E}(f_n) - AAL_0(f_n) \qquad (7)$$

describes the difference between the accumulated acceleration level [2] of the nth rocking mode $AAL_{n,E}$ and the AAL_0 of the fundamental mode. This measure can be applied to the total rocking mode considering all root causes (replacing subscript E by T) or to each contribution generated by the imbalance of mass, stiffness and force factor represented by symbol $E \in \{M,K,Bl\}$. A useful approximation of Eq. (7) is

$$RRL_{n,E}(f_n) \approx 20\log_{10}\left(\frac{\int_{S_c}|X_{n,E}(f_n,\mathbf{r}_c)|dS}{\int_{S_c}|X_0(f_n,\mathbf{r}_c)|dS}\right) \qquad (8)$$

using the displacement $X_{n,E}(f_n, \mathbf{r}_c)$ of the rocking modes and the displacement $X_0(f_n, \mathbf{r}_c)$ at the point $\mathbf{r}_c$ on the radiator's surface S_C. A value RRL which is larger than -5 dB indicates a significant rocking mode.

3.3 Assessing the Modal Resonators

The modal resonator generates based on excitation signal E_n with n=0,1,2 the modal state variables $\mathbf{x_L} = [x_0\ \tau_1\ \tau_2]^T$ as shown in Fig 1. The resonators of the two rocking modes behave like a narrow band pass filter *boosting* the excitation signal E_n at the particular resonance frequency f_n significantly. Although, the excitation $E_n(f)$ at frequencies f below and above the resonance frequencies f_n is not relevant for the generation of critical rocking behavior the frequency response of $E_n(f)$ was the basis for the identification of the free model parameters. In this section useful characteristics, which gives a deeper insight into the excitation process and the properties of the resonators are presented.

3.3.1 Modal Force Ratio $MFR_{n,E}$

The excitation signal E_n generating the nth-rocking mode are transformed into the equivalent modal forces

$$F_{n,T} = E_n / d_{ref} \qquad (9)$$

using a reference distance d_{ref} which corresponds with the diameter of the radiator's surface. Comparing those forces with the transversal force F_0 of the fundamental mode give the total modal force ratio in percent:

$$MFR_{n,T} = \frac{|F_0(f_n) + F_{n,T}(f_n)| - |F_0|(f_n)}{F_0(f_n)}100\% \qquad (10)$$

Considering the moments $\mu_{n,E}$ due to the imbalances mass, stiffness and force factor represented by subscript $E \in \{M,K,Bl\}$ gives the force component

$$F_{n,E} = \mu_{n,E} / d_{ref} \qquad (11)$$

and the modal force ratio of component E:

$$MFR_{n,E} = \frac{|F_0(f_n) + F_{n,E}(f_n)| - |F_0|(f_n)}{F_0(f_n)}100\% \qquad (12)$$

3.3.2 Combined Force Ratio CFR

Exploiting the orthogonal properties of the mode shapes the following approximation gives the magnitude of the combined total force considering all root causes

$$F'_T \approx \sqrt{F_{1,T}^2(f_m) + F_{2,T}^2(f_m)} \qquad (13)$$

at the geometrical mean frequency $f_m = \sqrt{f_1 f_2}$ located between the two resonances.

The total combined force ratio CFR_T considering the contribution of all imbalances

$$CFR_T = \frac{F'_T(f_m)}{F_0(f_m)}100\% \qquad (14)$$

compares the combined total force F'_T with the piston mode force F_0 at f_m.

Considering the contributions of mass, stiffness and force factor imbalance represented by subscript $E \in \{M,K,Bl\}$ gives the force components

$$F'_E \approx \sqrt{F_{1,E}^2(f_m) + F_{2,E}^2(f_m)} \qquad (15)$$

and the combined force ratio CFR_E of component E:

$$CFR_E = \frac{F'_E(f_m)}{F_0(f_m)}100\% \qquad (16)$$

The direction of the equivalent forces F'_T and F'_E can also described by angles β_T and β_E with $E \in \{M,K,Bl\}$ calculated by a vectorial summation of the two modal forces.

The angles β_E of the force components are directly related to the angles γ_E defined by the coordinates of the center of mass, stiffness and force factor in Eq. (6). The combined force ratio has higher diagnostic value than the distance d_E between center point and pivot point presented in Eq. (5) because the CFR also considers the particular excitation condition depending on the on location of the fundamental resonance f_0 and the mean frequency f_m.

3.3.3 Relative Resonator Gain

The transfer functions $H_n(s)$ of the resonators with n=1,2 depends on resonance frequency f_n, relative gain G_n and loss factor η_n as described in detail in [1] the total modal

force $F_{n,T}$ and the total accumulated acceleration level $AAL_{n,T}$ can be calculated as

$$RG_n = RRL_{n,T}(f_n) + 20\log_{10}\left(\left|\frac{F_0(f_n)}{F_{n,T}(f_n)}\right|\right) \quad (17)$$

this is a valuable characteristic to assess the behavior of each modal resonator with *n=1,2* at the natural frequency f_n. Clearly the transducer design is interested to keep the relative resonator gain as small as possible by maximizing the loss factor η_n, increasing the natural frequency of the rocking modes f_n by making the rotational stiffness of the suspension in the direction of the tilting angles as high as possible and reducing the moment of inertia involved in the rocking modes.

4. EVALUATION

The new measurement technique has been evaluated by numerical simulations (FEA) and experiments on a multitude of real transducers using laser vibrometry. The distribution of mass, stiffness and force factor are changed systematically by applying known perturbations on virtual and real transducers. This case study also illustrates the diagnostic value of the new measurement technique.

4.1 Numerical Evaluation

A Finite Element Analysis (FEA) has been used to calculate the total displacement $x(\mathbf{r}_c)$ on the surface of the radiator while considering a mass, stiffness or force factor imbalance. After identifying the model parameters, the combined force ratio (CFR) is calculated which indicates magnitude and direction of the excitation signal driving the modal resonator.

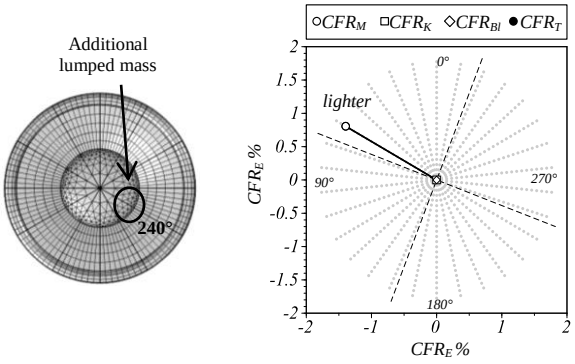

Fig 3. FE simulation of a rocking mode excited by a mass imbalance generated by additional lumped mass element (left), and the combined force ratio (right) revealing the total excitation (CFR_T) and the contribution (CFR_E) by the mass (M), stiffness (K) and force factor (Bl) imbalance

4.1.1 Mass imbalance

An additional mass element is placed at outside the pivot point at a position as depicted on the left-hand side of Fig 3. The parameter identification reveals the center of gravity shifted by d_M=0.3mm into the same direction at angle γ_M=240°. This imbalance generates a moment driving the first rocking resonator at the resonance frequency 300 Hz. The vector overlaid to the scanning grid on the right hand-side indicates the lighter side of the radiator which is exactly located on the opposite side of the center of gravity. The force ratio CFR_M*=1.6%* generated by the mass imbalance (M) only dominates the total force ratio CFR_T*=1.6%*.

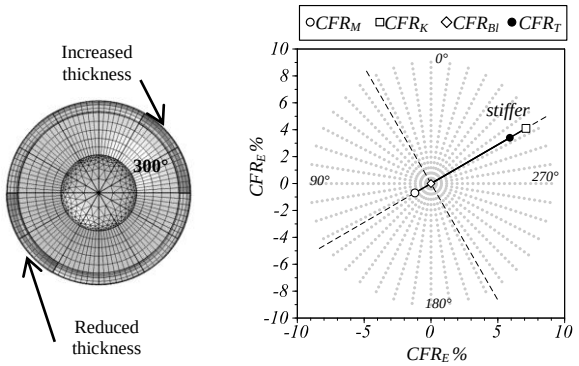

Fig 4. FE simulation of a rocking mode excited by a stiffness imbalance generated by varying thickness of the surround area (left) and the combined force ratio (right) revealing the total excitation (CFR_T) and the contribution (CFR_E) by the mass (M), stiffness (K) and force factor (Bl) imbalance

4.1.2 Stiffness imbalance

A stiffness imbalance was generated by varying the thickness of the surround over the circumference as shown in the left-hand side of Fig. 4. The parameter identification reveals the center of stiffness shifted by the distance d_K=1.07 and in the direction γ_K=300° from the pivot which agrees with the variation of the thickness. The vector displayed on the scanning grid on the right hand side of Fig 4 shows the stiffer side of the distribution, which also agrees with perturbation. The length of the vector represents the magnitude of the combined force ratio CFR_K *=8.2.%* which is the dominant contribution to the total force ratio CFR_T.

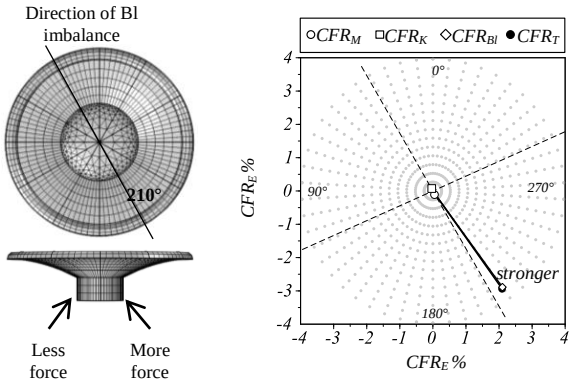

Fig 5. FE simulation of a rocking mode excited by a force factor imbalance (left) and the combined force ratio (right) revealing the total excitation (CFR_T) and the contribution (CFR_E) by the mass (M), stiffness (K) and force factor (Bl) imbalance

4.1.3 Force Factor Imbalance

A force factor imbalance was simulated by increasing and reducing the force factor on opposite sections of the voice coil as shown on the left-hand side in Fig 5. The center of force factor distribution has been identified at the distance d_{Bl}=3.1mm and in the direction γ_{Bl} =210° form the pivot point which agrees with introduced force factor imbalance. This vector on the left hand side represents the combined force ratio points into the same direction. The component CFR_{Bl} =3.5% contributed by the force factor imbalance coincides with the total ratio CFR_T indicating a dominant Bl imbalance.

4.2 Experimental Evaluation

In addition to FE simulations further experiments have been performed on real transducers modified by intentional perturbations. In order to ensure that the rocking mode is excited dominantly by the perturbation, the transducer was measured before and after each modification, but here only the results of the transducer will be presented.

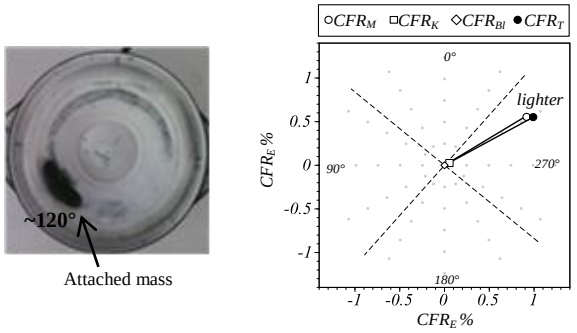

Fig 6. Combined force ratio *CFR* plotted over scanning grid (right) reveals the direction and magnitude of the combined excitation force generated by a mass perturbation (left).

4.2.1 Mass Perturbation

A mass imbalance was experimentally realized by attaching a small amount of clay close to the surround at a position shown on the left side in Fig 6. The rocking mode analysis reveals that this perturbation shifts the center of mass by d_M=0.24mm to the same direction γ_M =121°. The mass imbalance (white circle) generates the dominant contribution CFR_M=1.07% to the total the total force ratio (black circle) exciting primarily the first rocking mode. The direction of the combined excitation force agrees with the position of the perturbation and the identified center of gravity.

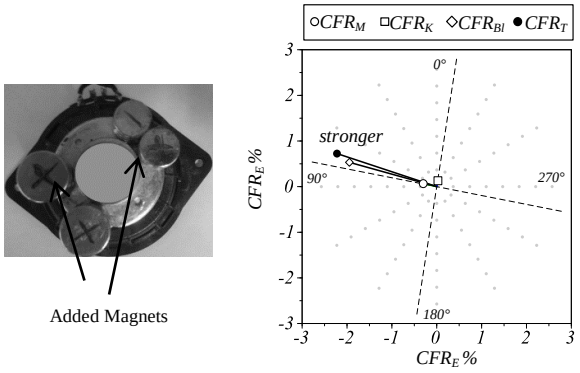

Fig 7. Combined force ratio *CFR* plotted over scanning grid (right) reveals the direction and magnitude of the combined excitation force generated by a force factor perturbation (left).

4.2.2 Force Factor Perturbation

A force factor imbalance was generated by attaching two arrays of axially polarized magnets on the back-plate as shown on the left-hand side of Fig 7. The rocking mode analysis shifts the center of force factor by distance d_{Bl}=1.69mm to the direction defined by angle γ_{Bl} =76°**.** The vector representing the total combined force ratio *CFR* (black circle) pointing to the same direction as shown on the left hand side of Fig 7. The contribution CFR_{Bl}=2.0% generated by *Bl* imbalance (rhomb) is the dominant root

cause which is increased by the contribution of mass (white circle) pointing to the same direction. The contribution of stiffness (square) is negligible.

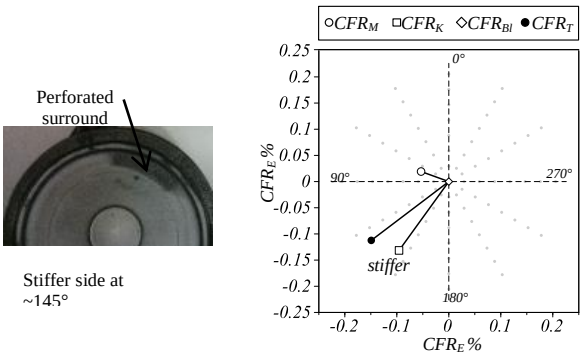

Fig 8. Combined force ratio *CFR* plotted over scanning grid (right) reveals the direction and magnitude of the combined excitation force generated by a stiffness perturbation (left).

4.2.3 Stiffness perturbation

A stiffness imbalance was generated by perforating a section of the surround by a pin without affecting significantly the mass distribution as shown on the left-hand side of Fig 6. The rocking mode analysis shifts the center of stiffness by d_K=1.02 mm to the direction defined by angle γ_K =143° which agrees with the direction of the perturbation. The right-hand side shows the stiffness imbalance (square) as the dominant contribution CFR_K=0.16% to the total force ratio (black circle). The vector points to the center of stiffness and the harder side of the surround. A small mass imbalance (circle) generating a much smaller contribution CFR_M=0.05% in perpendicular direction to the force generated by the stiffness imbalance.

5. *Transducer Diagnostics*

In the following section the rocking mode analysis will be applied to a transducer as used in headphones exhibiting visible rocking behavior in the laser scan. The modal analysis applied to the measured displacement is used to separate the rocking modes (n=1,2) from the fundamental mode (n=0) and to calculate the relative rocking level RRL in accordance with Eq. (7) shown in Table 1.

Relative Rocking Level *RRL(dB)*	Dominant (n=1)	Second (n=2)
Total contribution (*T*)	$RRL_{1,T}$ = 5.4	$RRL_{2,T}$ = -12.9
Mass Imbalance (*M*)	$RRL_{1,M}$ = -8.6	$RRL_{2,M}$ = -18.4
Stiffness Imbalance (*K*)	$RRL_{1,K}$ = 1.4	$RRL_{2,K}$ = -17.7
Force factor Imbalance (*Bl*)	$RRL_{1,Bl}$ = -9.6	$RRL_{2,Bl}$ = -12.6

Table 1. Relative Rocking Level (RRL) of the first and second rocking modes and the contribution by each root cause

The first mode at the natural frequency f_1=151 Hz has a total Relative Rocking Level $RRL_{1,T}$ =5.4 dB showing that the rocking mode generates an *AAL* which is higher than the desired piston mode. The rocking mode analysis reveals the contribution of the mass, stiffness and force factor imbalances. The dominant root cause is the stiffness imbalance (*K*) generating a contribution of $RRL_{1,K}$ =1.4 dB. The contributions generated by mass and force factor imbalances are -10 dB lower in the first rocking mode. The second rocking mode at the natural frequency f_2=129 Hz generates a much smaller value of the total $RRL_{2,T}$ =-12.9 dB. The 2nd rocking mode is almost not visible in the optical animation of the laser scanning data. Here the component generated by the force factor imbalance (Bl) provides the largest contribution.

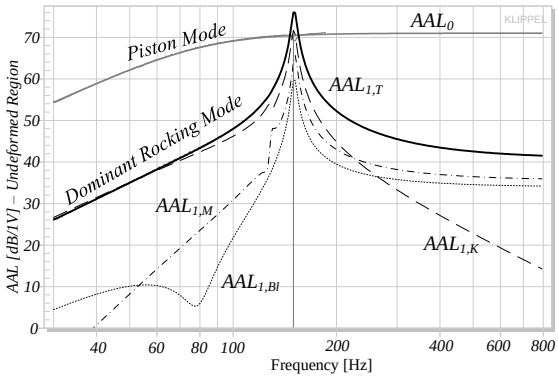

Fig 9. Accumulated acceleration level of the piston mode (AAL_0), the total 2nd rocking rocking mode ($AAL_{1,T}$) and the contributions ($AAL_{1,E}$) from the imbalances $E \in \{M,K,Bl\}$ versus frequency *f*

Fig 9. shows the total accumulated acceleration level $AAL_{1,T}$ of the first rocking mode versus frequency. The solid curve calculated by modal analysis based on the scanning data coincides almost perfectly with the dashed curve predicted by the modal model. This diagram also shows the contribution of each root cause. The $AAL_{1,K}$ generated by the stiffness imbalance (K) represented as the thick dashed curve shows the highest value at low frequencies but decays rapidly at frequencies above the resonance frequency f_1=151 Hz. The $AAL_{1,M}$ generated by the mass imbalance represented as the thin dashed curve stays constant at high frequencies but decays rapidly to lower frequencies. The frequency response of the $AAL_{1,Bl}$ generated by the force factor imbalance shows similar

slopes at very low and high frequencies as the responses of $AAL_{1,K}$ and $AAL_{1,M}$, respectively. However, the force factor imbalance generates a unique dip in the $AAL_{1,Bl}$ response at the fundamental resonance frequency f_0=80 Hz. Thus, the location of the rocking resonance frequencies f_n with n=1,2 with respect to the fundamental resonance frequency f_0 influences the relative rocking level $RRL(f_n)$. Assuming the imbalances of mass, stiffness and *Bl* would have the same center point then the stiffness would generate the lowest contribution $RRL_{n,K}$ to the total $RRL_{n,T}$ for resonance frequencies $f_n > f_0$. The mass imbalance would generate the smallest contribution $RRL_{n,M}$ at frequencies $f_n < f_0$ and *Bl* imbalance give the smallest contribution $RRL_{n,Bl}$ for $f_n = f_0$. With the assumption above the mass imbalance reduces the effect of the other contribution from stiffness and Bl imbalance at resonance frequencies $f_n > f_0$.

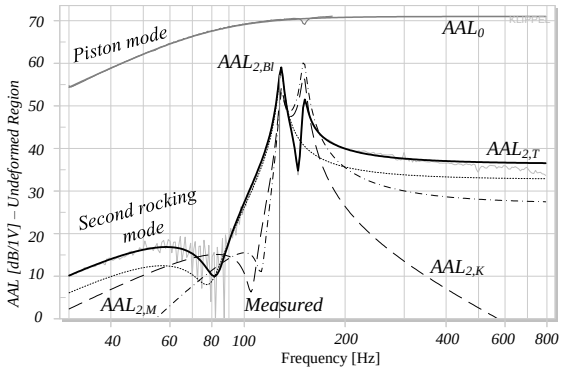

Fig 10. Accumulated acceleration level of the piston mode (AAL_0) , the total 2nd rocking rocking mode ($AAL_{2,T}$) and the contributions ($AAL_{2,E}$) from the imbalances $E \in \{M,K,Bl\}$

Fig 10. shows the accumulated acceleration level $AAL_{2,T}$ of the second rocking mode calculated by modal analysis based on measured displacement (thin solid line) and predicted by the modal model (thick solid line). Both curves agree at high *AAL* values where the measurement noise is negligible. The total $AAL_{2,T}$ of the second rocking mode reveals two peaks corresponding with the natural frequencies f_n of the rocking resonators n=1,2. While the peak at the lower frequency f_2=*129 Hz* corresponds with natural frequency of the 2nd mode, the peak at higher frequency f_1=*151 Hz* is generated by coupling with the first mode (secondary excitation).

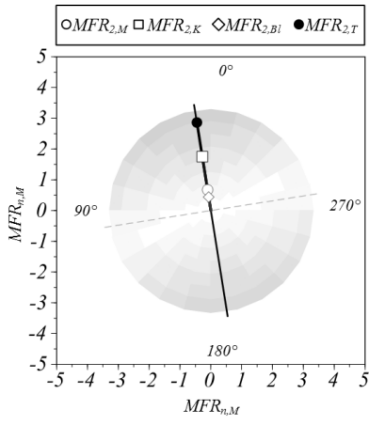

Fig 11. Modal Force Ratio MFR_1 describing the excitation of the first rocking mode of the headphone

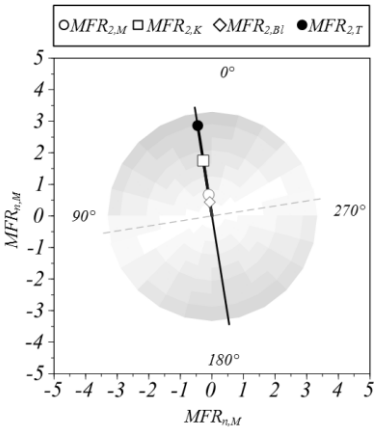

Fig 12. Excitation Ratio MFR_2 describing the exciation of the second rocking mode of the headphone

Fig 11 and Fig. 12 show the mode shapes of the first and second rocking mode where thin dashed lines indicate the nodal lines. The vector ending with the black circle represents the modal excitation ratio $MFR_{n,T}$ with n=1,2 considering all root causes. The vectors ending with other symbols represent the contributions $MFR_{n,E}$ with $E \in \{M,K,Bl\}$ of the mass, stiffness and Bl imbalance.

Modal Force Ratio	First mode ($n=1$) in %	Second mode ($n=2$) in %
Total (*M,K,Bl*)	$MFR_{1,T}$ =2.9	$MFR_{2,T}$ =0.57
Mass (*M*)	$MFR_{1,M}$ =0.68	$MFR_{2,M}$ =-0.24
Stiffness (*K*)	$MFR_{1,K}$ = 1.77	$MFR_{2,K}$ =-0.29
Force factor (*Bl*)	$MFR_{1,BL}$ = 0.44	$MFR_{2,Bl}$ =0.53

Table 2. Total force ratio and the contributions from mass, stiffness and Bl imbalances.

Table 2 shows the values of the modal force ratios where the magnitude corresponds with the length of the vector and the sign with the direction of the vectors in Fig 11 and Fig. 12. The positive values $MFR_{1,E}$ of all components $E \in \{M,K,Bl\}$ indicate that all imbalances contribute constructively to the first rocking mode.

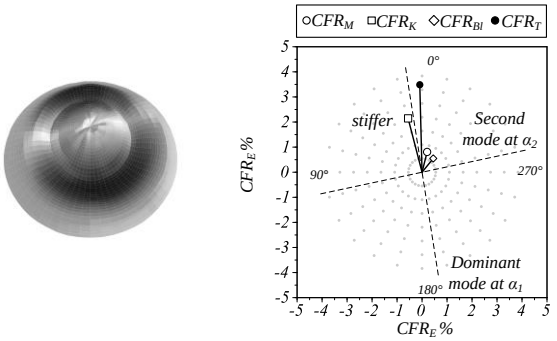

Fig 13. Mode shape of the first rocking mode (left) and the vectors representing the combined force ratio and the contribution by mass, stiffness and force (right)

Imbalance	Characteristics	Value
Mass (M)	CFR_M	0.83 %
	β_M	345.9°
Stiffness (K)	CFR_K	2.22 %
	β_K	14.6°
Force factor (Bl)	CFR_{Bl}	0.71 %
	β_{Bl}	320.8°
Total (M,K,Bl)	CFR_T	3.49%
	β_T	1.5°

Table 3. Combined force ratio CFR_E and angle β_E indicating the magnitude and direction of the excitation of the rocking modes by the imbalance E

The total combined force ratios CFR_T and the angle β_T presented in Table 3 show the magnitude and direction of the force exciting both rocking resonators. The directions of the vectors representing the contributions CFR_E of each imbalance $E \in \{M,K,Bl,T\}$ are closely related to the center of gravity, stiffness and force factor as shown in Table 4.

Center of	Coordinates	Value
Gravity (M)	d_M	0.08 mm
	γ_M	168°
Stiffness (K)	d_K	0.73 mm
	γ_K	17.54°
Force factor (Bl)	d_{Bl}	0.9 mm
	γ_{Bl}	320°

Table 4.Polar coordinates of the center of gravity (M), stiffness (K) and force factor (Bl) identified by the modal modelling of the headphone transducer.

However, the combined force ratio has a higher diagnostic value then the coordinates d_E and γ_E of the center points because this characteristic also considers the influence of the resonance frequencies f_n with n=0,1,2 on the excitation of the modal resonators.

The CFR values in percent are presented as vectors on the scanning grid in Fig 13. The stiffness imbalance generates the largest contribution CFR_K (square) to the total CFR_T (black circle) located at angle β_T close to the angle α_1 of the first mode. The force factor imbalance (rhomb) is located at angle β_{Bl} which also excites the second mode represented by angle α_2. The angle β_K and β_{Bl} of the vectors of the contribution are almost identical with the angles γ_K and γ_{Bl} of the center point of the stiffness and Bl distribution, respectively. The angles of the mass imbalance are related by $\beta_M \approx \gamma_M+180°$ due to the particular excitation condition of the mass imbalance for frequencies $f_n > f_0$ with n=1,2.

Modal resonator *(n=1,2)*	First mode *(n=1)*	Second mode *(n=2)*
Resonance frequency	f_1 = 151 Hz	f_2 = 129 Hz
Relative gain at f_n	RG_1= 36 dB	RG_2= 31.6 dB
Loss factor	η_1 = 0.016	η_2= 0.014
Quality factor	Q_1 = 30.2	Q_2 = 34.7

Table 5. Characteristics of the rocking resonators

After investigating the excitation condition the characteristics of the rocking resonators given in Table 5 are discussed in greater detail. The high quality factors Q_n of the rocking modes n=1,2 generate a high gain RG_n and a peaky shape of the rocking resonance as shown in Fig 9 and Fig 10. The mechanical losses damping the rocking modes are much smaller than the mechanical losses damping the fundamental piston mode. The tilting of the diaphragm pushes the air from one side to the other side of the rotational axis while the piston mode presses the air through the magnetic gap where turbulences generate significant losses. Although the headphone transducer uses an axial-symmetrical (round) diaphragm, the litz wires and irregularities in the mass and stiffness distribution generate a significant difference between the two resonance frequencies f_1 and f_2.

In order to separate systematic and random root causes it is strongly recommended to scan a second unit of the same transducer type. If the rocking mode analysis shows a dominant stiffness imbalance at the same location, the constructional causes for the imbalances should be searched in the design and production process. Random problems may be caused by varying properties (thickness) of the raw material used for the diaphragms and suspension. All activities should be focused on removing the dominant imbalance, in the particular example the stiffness distribution. Increasing the rotational stiffness would also reduce the relative rocking level generated by all three imbalances because the higher rocking resonance frequencies ($f_1 > f_s$) impairs the excitation condition for a stiffness imbalance. However, increasing the rotational stiffness in headphone and micro-speakers will also increase the translational stiffness K_{ms} and the fundamental resonance frequency f_s. In woofers a larger rotational stiffness can be realized by increasing the distance between spider and surround while keeping the total stiffness K_{ms} constant. To reduce the quality factor of the rocking modes the loss factor in the material used for suspension and diaphragm should be increased.

6. CONCLUSIONS

The new measurement technique analyses the excitation and vibration of rocking modes based on an extended model using lumped parameters in the modal space. The free parameters of the model are identified for the particular transducer based on measured displacement easily accessible by laser vibrometry. Further characteristics simplify the interpretation of the basic model parameters and give a deeper insight into the excitation of the modal resonators. This is the basis to localize and assess the magnitude of imbalance which is the difference (in mm) between the center point in the mass, stiffness and force factor distribution and the cross point between the nodal lines (pivot point). Although this difference is the actual root cause of the rocking behavior the amplitude of the rocking mode depends also on excitation conditions and the gain of the rocking resonators. Due to the high quality factor of the rocking resonators only a very small asymmetrical force is required (which is usually a few percent of the transversal force) to generate a critical rocking behavior having more energy than the desired piston mode. Assessing the relative rocking level RRL and identifying the imbalances is a convenient way to keep voice coil rubbing under control and to avoid impulsive distortion impairing the quality of the reproduced sound.

7. REFERENCES

[1] W. Cardenas and W. Klippel, "Loudspeaker Rocking Modes (Part 1: Modeling), presented at the 139th Convention of the Audio Eng. Soc. 2015 October 29–November 1 New York, USA

[2] Klippel, Schlechter, "Distributed Mechanical Parameters of Loudspeakers, Part 1: Measurements", Journal of Audio Eng. Soc. Vol. 57, No. 7/8, 2009 July/August, pp. 500 – 511

[3] A. Bright, "Vibration Behaviour of Single-Suspension Electrodynamic Loudspeakers", presented at the 109th Convention of the Audio Eng. Soc., Los Angeles, CA, USA, 2000 September 22-25

[4] N. W. McLachlan, Loud Speakers, Theory, Performance, Testing, and Design. pp. 69 – 72. Oxford University Press, London, U. K. (1934).

[5] W. Klippel, J. Schlechter, „Distributed Mechanical Parameters of Loudspeakers, Part 2: Diagnostics", Journal of Audio Eng. Soc. Vol. 57, No. 9, 2009 , pp. 696 – 708